The Effects of pH and Temperature on Electrodeposition of Re-Ir-Ni Coatings from Aqueous Solutions

Wangping Wu,[a] Noam Eliaz,[a,*,z] and Eliezer Gileadi[b,]**

[a]*Biomaterials and Corrosion Laboratory, Department of Materials Science and Engineering, Faculty of Engineering, Tel-Aviv University, Ramat Aviv 6997801, Israel*
[b]*School of Chemistry, Faculty of Exact Sciences, Tel-Aviv University, Ramat Aviv 6997801, Israel*

The Re-Ir system is of great interest for high-temperature applications and extreme environments. Here, Re-Ir-Ni alloy coatings were electroplated from aqueous solutions. The effects of pH and temperature on the faradaic efficiency (FE), chemical composition, surface morphology and crystallographic structure of the coatings were studied. The results show that the pH and temperature of electrolytes have a significant effect on the electrodeposition of Re-Ir-Ni. As the pH was increased from 2.0 to 8.0, the FE, partial current densities for deposition of the three metals, and deposition rate increased. The highest Re-content (82 at%) was obtained at pH = 2.5. At pH = 2.0, the coating consisted of an amorphous phase, and no cracking was observed. When raising the pH to 4.0 and above, crystalline phases (including hydrides) formed, and both columnar crystals and micro-cracks were observed. The bath temperature affected the surface crack density and the size of the grains that form the mesoscopic colonies. At the two lowest temperatures studied herein (50 and 60°C), no codeposition of Ir was observed. The phase composition of the coating changed from amorphous Re-Ni at 50°C; to amorphous Re-Ni, hcp-Ni and hexagonal Ni_2H at 60°C; to hcp-$Ir_{0.4}Re_{0.6}$, hcp-Ni and hexagonal Ni_2H at higher temperatures.
 [DOI: 10.1149/2.0281501jes]

Manuscript submitted September 15, 2014; revised manuscript received October 27, 2014. Published November 8, 2014.

Pure rhenium (Re) has high melting point (3,186°C), excellent wear resistance, and superior strength and ductility at elevated temperatures. In addition, it does not suffer from ductile-to-brittle transition, and it does not form carbides while having good mutual wettability with carbon.[1,2]

At present, the main manufacturing processes of Re and its alloys are powder metallurgy and chemical vapor deposition (CVD).[1–3] In recent years, we have studied electroplating[4–12] and electroless plating[13,14] as alternative processes. Electrodeposition of pure Re was found to have a low faradaic efficiency (FE) and poor quality.[4] Addition of iron-group metal salts to the plating bath results in the formation of Re-Me alloys (Me = Ni, Co or Fe) with high Re-content and at high FE, thus showing a catalytic effect of the iron-group metals on the electrodeposition of Re.[5,7]

Rhenium and its alloys with iron-group metals tend to oxidize readily in moist air at temperatures above 600°C.[1,2] In order to protect them from high-temperature oxidation, a top coating such as rhodium (Rh) or iridium (Ir) is often applied. Iridium has high melting point (2,446°C) and excellent corrosion resistance.[15,16] Re and Ir show extensive mutual solubility and no intermetallic compounds in their binary phase diagram. Iridium can also act as an effective diffusion barrier for inward-diffusing oxygen and outward-diffusing carbon. It is thus one of the most promising candidates for protective coating of either structural carbons or Re-based components for extreme environments.[2,17,18] Iridium-coated Re nozzles are used in aerospace applications for small chemical rockets and resistojet thrusters.[19] A combustion chamber composed of Re substrate and Ir coating has been demonstrated to be stable for extended lifetimes at temperatures as high as 2,200°C.[20,21] NASA has reported the development of Ir-coated Re rocket chamber technology, allowing an increase in satellite life from 12 to 15 years, and gaining 30–60 M$ in the added revenue per satellite.[22]

Reed et al.[20] have claimed that CVD is the only established process for the fabrication of Ir-coated Re combustion chambers. However, some aspects such as high costs, low deposition rates, high deposition temperature and impurity incorporation into the films are of major concern.[23] Other manufacturing processes for Ir and its alloys include physical vapor deposition (PVD)[24,25] and electrodeposition.[26–28] The electroplating of pure Ir from aqueous solutions has some disadvantages with respect to the stability of electrolyte and quality of deposits.[29] Significant hydrogen evolution might lead to deterioration of the Ir deposits, cracking and low FE.[30]

In our group, Cohen Sagiv et al.[9] developed suitable plating baths for electroplating of Re-Ir-Ni coatings, suggested a mechanism for the deposition process, and determined the effect of plating bath chemistry and operating conditions on the uniformity, thickness, chemical and phase composition of these coatings. The deposition was done from aqueous citrate solutions under galvanostatic conditions ($j = 50$ mA cm^{-2}) at pH = 5.0 and $T = 70$°C. Re-Ir-Ni coatings as thick as 18 μm, with Re-content as high as 73 at% and Ir-content as high as 29 at%, were obtained.

Recently, we have identified a combination of a multilayer and columnar structure in Re-Ir-Ni coatings. Furthermore, an indication was found, that the pH might affect the structure of the deposits and their surface cracking pattern [unpublished data]. In addition, in order to achieve the maximal service temperature of the coatings, there is interest in further increasing their Re-content. It is well known that the variation of pH in citrate-containing perrhenate (and other) electroplating baths results in the formation of different metal-citrate complexes, which is expected to have an impact on the overall electroplating process and the nature of the deposits.[31–33] The temperature of the electrolytes is another important parameter in electroplating of Re-based alloys.[1,31] Thus, the objective of the current study was to investigate the effects of pH and temperature on the FE, surface morphology, chemical composition, and crystallographic structure of electrodeposited Re-Ir-Ni ternary alloys.

Experimental

A small three-electrode cell was used. It consisted of a copper (Cu) disc cathode with an exposed surface area of 1.57 cm^2 serving as the working electrode (WE), two platinum sheets placed at about 0.5 cm away on both sides of the WE and serving as the counter-electrode (CE), and a Ag/AgCl/KCl(sat.) reference electrode (RE). Prior to electroplating, the surface of the Cu substrate was cleaned with soap solution in an ultrasonic bath for 5 min in order to remove major contaminants, and then immersed in a 1:1 by volume (nitric acid (70%) : deionized water) at room temperature for about 1 min, to remove the native oxide films on the surface of the Cu substrate. This was followed by another cleaning with acetone in an ultrasonic bath for 3–5 min. The bath chemistry and operating conditions for electrodeposition of Re-Ir-Ni alloys are listed in Table I. All solutions were dissolved

*Electrochemical Society Active Member.
**Electrochemical Society Fellow.
zE-mail: neliaz@eng.tau.ac.il

Table I. Bath chemistry and deposition conditions.

Bath chemistry		Deposition conditions	
NH_4ReO_4 (mM)	35	pH	(2.0–8.0) ± 0.1
$IrCl_3 \cdot nH_2O$ (mM)	35	Temperature (°C)	(50–90) ± 1
$Ni(NH_2SO_3)_2 \cdot 4H_2O$ (mM)	35	Current density (mA cm^{-2})	50
$C_6H_8O_7$ (mM)	35	Deposition time (h)	1

in deionized water (Simplicity, Millipore). The pH of the solution was measured by pH meter 510 from Eutech Instruments, and was adjusted to the desired value by adding 5.0 M sodium hydroxide solution at room temperature. A Princeton Applied Research model 263A Potentiostat/Galvanostat was used to control the applied current density. A MRC B300 thermostatic bath was used to control the bath temperature. The bath was purged with pure nitrogen for at least 15 min before turning on the current. A nitrogen blanket was used during deposition. A magnetic stir bar was used to stir the solution, in order to maintain homogeneity of the solution and reduce pitting.

The mass gain due to coating formation was measured by a BA 210 (Sartorius) analytical balance (resolution 0.1 mg) before and after each experiment. The average FE was calculated from the added mass, the charge passed, and the chemical composition of the alloy. The partial current densities for the three metals and the thickness of the alloy coatings were calculated from the added mass and the chemical composition of the alloy. Further details can be found in our previous publication.[9]

The microstructure and morphology of both the top surface and a cross-section of a freshly fractured surface of the deposits were observed by an environmental scanning electron microscope (ESEM, Quanta 200 FEG, FEI) operated in the high-vacuum mode. The chemical composition of the alloy was determined by the attached liquid-nitrogen-cooled Oxford Si X-ray energy dispersive spectroscopy (EDS) detector. Each sample was tested at five locations, to confirm uniformity and present representative average values. The phase content of the alloy was determined by X-ray diffraction (XRD, Scintag, USA) equipped with a liquid-nitrogen-cooled germanium solid-state detector and a Cu-Kα radiation source. The as-deposited samples were cut mechanically to reveal the microstructure and measure the thickness of the coating.

Results and Discussion

The effect of pH.— The pH was varied from 2.0 to 8.0 while keeping the temperature (at 70°C) and all other variables constant. The characteristics of as-deposited samples are shown in Table II. The FE, added mass and deposition rate increased with increasing electrolyte pH. The FE, gained mass and deposition rate were the lowest at pH 2.0. An increase of pH, to 2.5, resulted in significant mass gain. At this pH, the Re-content was maximal and the Ni-content was minimal, which is desired for high-temperature applications. This is also an improvement compared to our previous publication,[9] in which the best sample contained 73 at% Re, 1 at% Ir and 26 at% Ni (although it was 11 μm thick). However, when decreasing the pH to 2.0, the Ir-content increases significantly whereas the Ni-content increases only slightly, at the price of decrease in the Re-content. It would be interesting to compare experimentally the high-temperature behavior of these two alloys and choose the one that provides the best combination of service temperature and oxidation resistance. For pH higher than 2.5, from Table II, opposite trends in the Re-content and in the FE are evident – as one increases, the other decreases. We have reported similar trends for electroplating of Re with iron-group metals.[5,7]

Figure 1 shows the effects of pH on the partial current densities of the three metals as well as of the hydrogen evolution reaction, the

Table II. Characteristics of as-deposited coatings as a function of pH.

pH	*w* (mg)	Re (at%)	Ir (at%)	Ni (at%)	FE (%)	*h* (μm)
2.0	3.8	70	18	12	4.3	1.2
2.5	12.2	82	8	10	15	3.8
3.0	17.5	64	7	29	21	6.1
3.5	17.6	64	6	30	21	6.2
4.0	29.2	38	14	48	32	11.4
6.0	34.8	31	14	55	38	14.3
8.0	39.7	33	13	54	44	16.3

Note: Bath temperature $T = 70°C$, deposition time 1 h. *w* is the gained mass, *h* is the thickness of the coating.

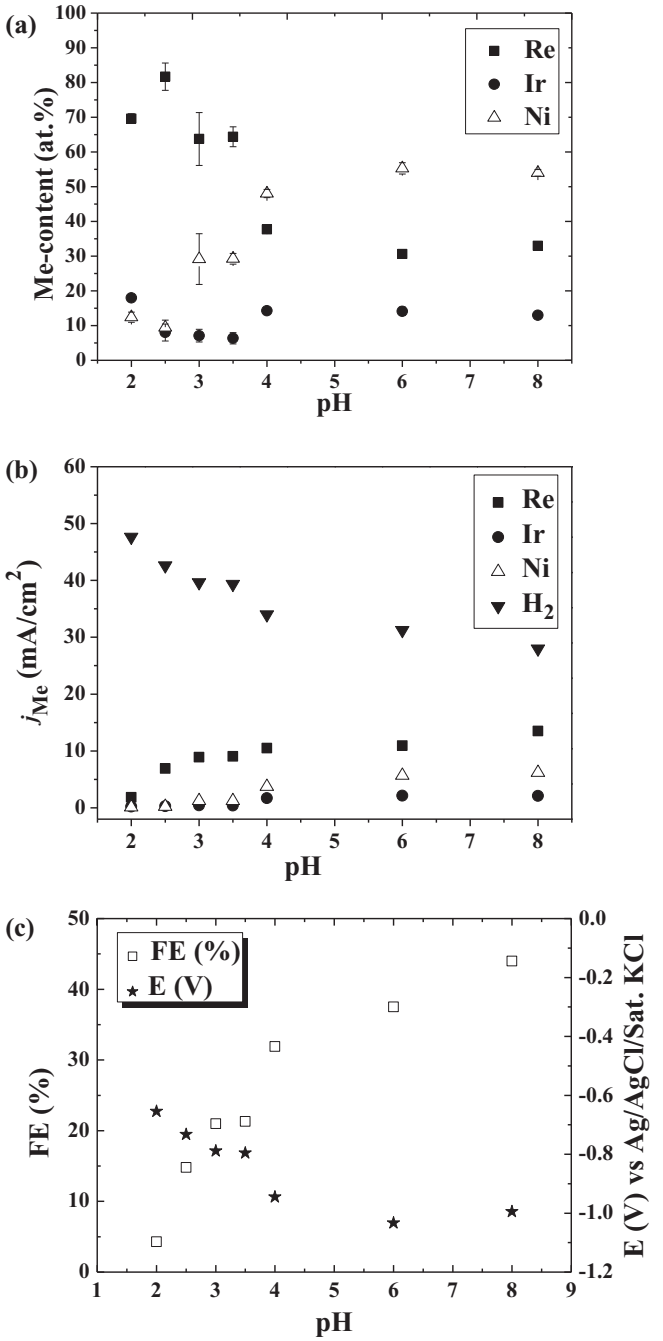

Figure 1. The effect of pH on the Me-content in the deposit (a), the partial current densities (b), the FE and the measured potential (c).

concentrations of the three metals in the alloy coating, the FE and the measured potential. From Fig. 1a it is evident that the highest Re-content (82 at%) was obtained at pH 2.5, but that at this pH the Ir-content in the alloy was rather low (8 at%). The FE is seen to increase from 4.3 to 15% as the pH changes from 2.0 to 2.5, thus a pH of 2.5 may be preferred industrially. Netherton and Holt[31] reported that the Re-content in Re-Ni alloys remained nearly constant for pH values between 3.0 and 8.0. In the current study, the Re-Ir-Ni alloys had a different behavior compared to the Re-Ni alloys. Considering the perrhenate-citrate complex $[ReO_4H_2Cit]^{2-}$, its dissociation rate was found to be independent of pH in the range of 3.0–5.5, but increased rapidly with decreasing pH below 3.0, approaching a first-order dependency at pH = 2.0.[33] We thus hypothesize that this complex being less stable at pH 2.0 or 2.5 allowed efficient plating of the alloy, which resulted in an increase in the Re-content and, correspondingly, low FE.

In Fig. 1b, the partial current densities for deposition of the three elements increased with increasing pH. The partial current density for hydrogen evolution decreased with increasing pH. It should be borne in mind that both Re and Ir are much better catalysts for hydrogen evolution than Ni, so that lowering the proportion of Re or Ir in the alloy would result in a decrease in the hydrogen evolution rate and, consequently, an increase of the FE. Indeed, in Fig. 1c it is evident that the FE increased with increasing pH. The measured cathodic potential increased by 0.35 V (from –0.65 to –1.0 V) as the pH was increased by 6 units (from 2.0 to 8.0). This variation corresponds well to the change of the reversible potential for hydrogen evolution according to the Nernst equation.

The effect of pH can be discussed with respect to the species derived from citric acid and their variation as a function of pH. At pH = 2.0, the predominant species is the neutral citric acid, while at pH = 8.0 it is the Cit^{3-} ion, which can form complexes with the two positive ions Ni^{2+} and Ir^{3+}. Since the total concentration of all citrate species at any pH is only one-half of the $(Ni^{2+} + Ir^{3+})$ concentration, there must be some free (hydrated) positive ions in solution. Increasing the concentration of citric acid to be at least equal to, or larger than, the sum of the concentrations of the above two positive ions may have interesting effects on the characteristics of electrodeposition and the properties of the coatings. This, however, will be the subject of another study. In Table II, we note a sharp increase in the FE between pH 2.0 and 4.0, which is probably due to the lower rate of the hydrogen evolution from a neutral citric acid molecule than from a free proton (H_3O^+).

Figure 2 displays the ESEM images of the top surfaces and fracture surfaces of Re-Ir-Ni coatings deposited at different pH values. At pH 2.0 (Fig. 2a), the surface of the alloy is dense and rough. There seem to be many small particles, but no visible micro-cracks. The fracture surface shows that the coating is relatively thin, with no evidence of grain boundaries (see Fig. 2b). In the range of pH 2.5–3.5, the surface of the coating was smooth and with only few fine micro-cracks, as observed by ESEM. When the pH was increased from 4.0 to 8.0, a network of micro-cracks appeared at the surface (see Fig. 2c, 2e and 2g). A closer examination revealed that the density of micro-cracks slightly increased with increasing pH. From the corresponding cross-section fracture images (Fig. 2d, 2f and 2h) it seems that some of the surface cracks actually penetrate through the thickness of the coating. This might be detrimental in terms of corrosion resistance. However, it cannot be excluded that some crack propagation occurred during the aggressive mechanical action of cutting. Both the top surfaces and the cross-section fracture surfaces of samples deposited at pH of 4.0, 6.0 and 8.0 look significantly different that those of the sample deposited at pH 2.0.

At the top surface (Fig. 2a, 2c, 2e and 2g), a mesoscale colony (or nodular) structure is evident, with clear intercolony boundaries and surface grooves. The appearance of these 3D islands indicates a Volmer-Weber (VW) growth mode.[34,35] This growth mode is preferred, regardless of the crystallographic misfit between the substrate and the deposit, when the binding energy between adsorbed deposited ions is greater than the binding energy between an adsorbed ion and a substrate atom. The formation of nodules (colonies) may be the outcome of nucleation extending laterally from an existing structural defect (e.g. dislocation) and sweeping deposit substances ahead of the growth front of film.

In the cross-section (Fig. 2d, 2f and 2h), a columnar crystal growth is evident, and the thickness of the coating looks uniform. However, in particular at pH 6.0 and 8.0, it seems that the coating actually consists of at least two parallel sublayers of similar thickness but somewhat different grain size. Coating delamination from the substrate, which is observed in Fig. 2b, 2f and 2h, was the outcome of the aggressive external mechanical force. These micro-cracks may result from volumetric changes due to hydrogen absorption during electroplating, from hydride decomposition shortly after electroplating, or from residual stresses due to formation of several phases with different lattice parameters within the coating.[1,9] In our previous publication,[9] the surface morphology of the Re-Ir-Ni coating was found to depend on the bath composition and operating conditions, and a network of micro-cracks was observed in all cases at pH 5.0. In the current study, few micro-cracks were present on the surface when the pH was in the range of 2.0–3.5, while the FE was low. Therefore, the cracking phenomenon is most likely not associated with hydrogen, but rather with the formation of different phases with different crystallographic structure, lattice parameters and volume. This conclusion is supported by the recent results of Rosen et al.[12] for pulse plating.

Columnar structures are characteristic of deposits from additive-free solutions, which are formed at a low deposition rate or elevated temperature. They are typically characterized by lower tensile strength and microhardness than other structures, but are generally more ductile and have high purity and density and small electrical resistivity.[36–38] Reddy[39] suggested, for columnar growth during electrodeposition of Ni, that adsorption of hydrogen atoms on the cathode surface should affect the texture of the coating.

The effect of pH on the crystallographic structure of the coating is shown in Fig. 3. For pH = 2.0 (see Fig. 3a), strong (111), (200), (220) and (311) reflections from the Cu substrate are apparent (JCPDS file #04–0836), thus indicating a thin deposit. A broad halo at ~42° indicates that the coating is composed of an amorphous phase. When the bath pH was increased to 4.0 and above (see Fig. 3b–3d), the reflections from the Cu substrate disappeared, thus indicating thicker coatings. In addition, new reflections, possibly related to crystalline $Ir_{0.4}Re_{0.6}$ and Ni_2H, appeared, in agreement with our past publication.[9] The co-existence of a Ni-rich crystalline phase is also evident. This phase may be the outcome of phase separation. The diffraction peak at ~40° indicates that these coatings consist of fine crystallites, although some peak broadening may be associated with inhomogeneities in the composition of the alloy or with micro-strain. The crystallite size is approximately 10 nm based on the XRD data. Complementary transmission electron microscopy (TEM) analysis is currently undertaken.

The effect of bath temperature.— The temperature of the electrolyte was changed between 50 and 90°C while keeping the pH (8.0) and all other variables constant. The effects of temperature on the characteristics of as-deposited samples are shown in Table III. The added mass and the deposition rate increased with increasing temperatures from 50 to 60°C, but then remained nearly constant. The increase of temperature could increase the rate of diffusion, as well as the rate of charge transfer. However, since the system probably contains different complexes, the equilibrium constant could also change with the increase of temperature. The extent of adsorption on the surface is also known to be a function of temperature, so that the overall effect can be measured, but is very hard to predict. In any case, at $T = 90°C$ the vaporization of the electrolyte was accelerated, which led to the degeneration of the electrolyte.

Figure 4 shows the effect of temperature on the partial current densities of the three metals as well as of the hydrogen evolution reaction, the concentrations of the three metals in the alloy coating, the FE and the measured potential. At $T = 50°C$ and 60°C, the coatings contained essentially no Ir (see Fig. 4a). The low deposition temperature resulted in a more negative deposition overpotential (see Fig. 4c), at which Ir

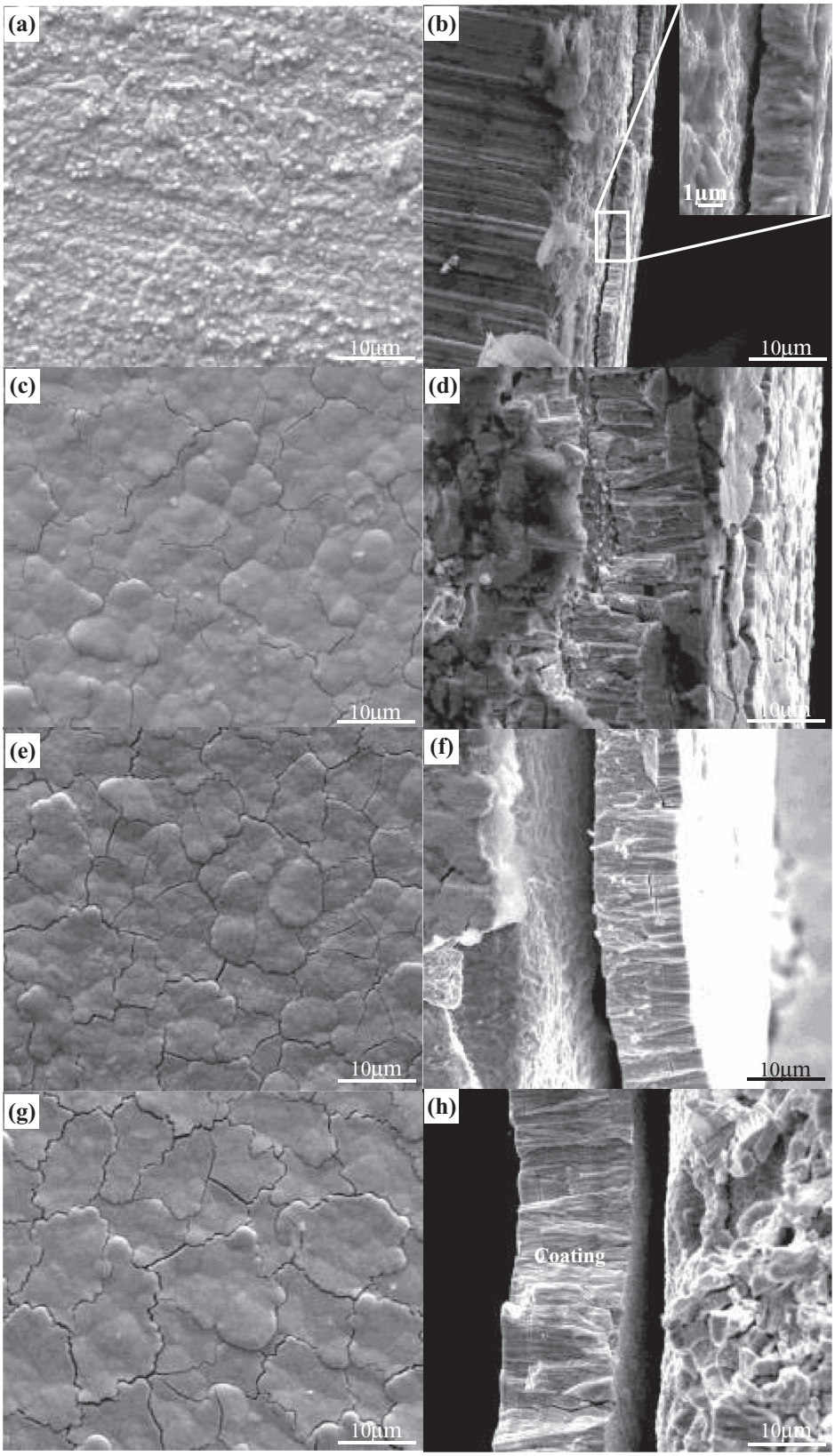

Figure 2. ESEM images of the top surfaces and fracture surfaces of Re-Ir-Ni coatings deposited at different pH values. (a, b) pH = 2.0, (c, d) pH = 4.0, (e, f) pH = 6.0, (g, h) pH = 8.0. The temperature was 70°C.

cannot be deposited from Ir^{3+} ions in alkaline aqueous solutions. At the higher temperatures used, the atomic composition of Ir increased to a constant value of 13–14 at%. The Ni-content behaved similarly, jumping from a nominal value of 42 at% at the two lower temperatures to around 54 at% at the higher temperatures. The Re-content changes in the opposite direction: higher at the lower temperatures, and lower at the three higher temperatures. Notably, the sum of (Ir + Re)-content was less dependent on temperature, having an average value of 58 at% at the two lower temperatures and 47 at% at the three higher temperatures. At $T = 70°C$, where most of our measurements

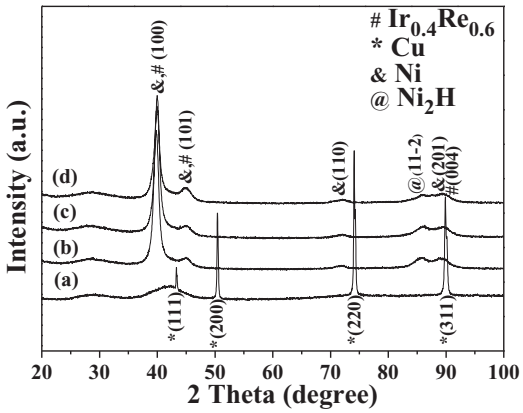

Figure 3. XRD patterns from Re-Ir-Ni coatings deposited at different pH. (a) pH = 2.0, (b) pH = 4.0, (c) pH = 6.0, and (d) pH = 8.0.

had been made, the sum of Re and Ir concentrations is 46 at%, and the Ni concentration is the highest (54 at%). The partial current densities for Re and Ni increased when the temperature was increased from 50 to 60°C (see Fig. 4b). With further increasing temperature, the partial current density of Re deposition decreased, reaching a steady value. In contrast, the partial current density of Ni deposition kept increasing to a nearly constant value. In Fig. 4c, the change of FE seems to be complex. When the temperature was 60°C, the FE reached a maximum value of 48%. The measured cathodic potential shifted to less negative values with increasing bath temperature, suggesting that the overpotential needed to start the electrodeposition process of the alloy is lower at higher temperatures, which is in accordance with the Nernst equation.

Figure 5 shows the ESEM images of the top surfaces and fracture surfaces of Re-Ir-Ni coatings deposited at different temperatures. At low temperature of 50°C, a mesoscale colony structure with large micro-cracks is seen on the surface (see Fig. 5a). A fine columnar structure was observed at the cross-section (see Fig. 5b). When the bath temperature was raised to 60°C, the crack density increased but their width decreased (Fig. 5c). The (hundreds of small) grains that form each colony became coarser. The columnar grains, which grow perpendicular to the surface of the substrate, also became coarser (see Fig. 5d). When the bath temperature was further raised to 70°C, the surface crack density increased significantly and the grains that form the colonies seemed to be finer (Fig. 2g), although the columnar grains at the cross-section did not seem to change significantly (Fig. 2h). With further increase of temperature to 80°C, the crack density increased even further and the grains within the colonies became smaller (Fig. 5e). The columnar structure along the thickness of the coating was still evident (Fig. 5f). Finally, when the bath temperature was raised to 90°C, the crack density decreased and the grains within the colonies became coarser (Fig. 5g). The columnar grains in the cross-section became coarser too (Fig. 5h). In all cases, the thickness of the coating was quite uniform.

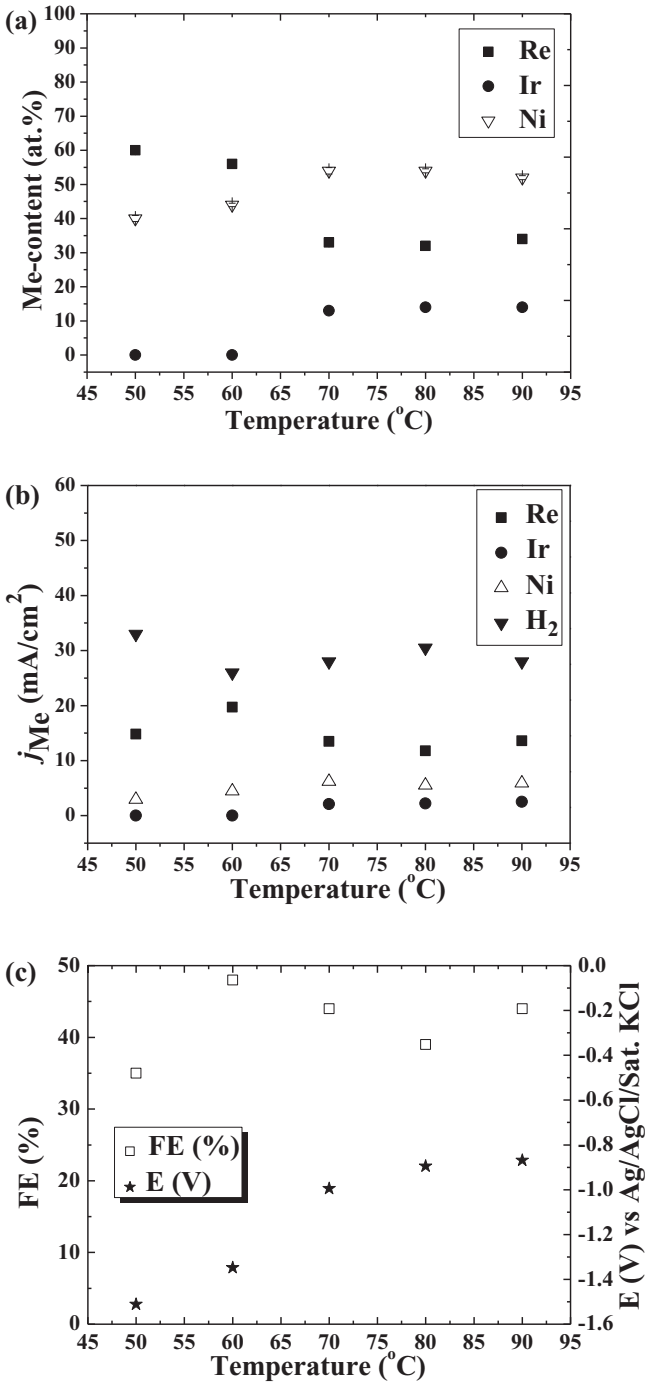

Figure 4. The effect of temperature on the Me-content in the deposit (a), the partial current densities (b), the FE and the measured potential (c).

Table III. Characteristics of as-deposited coatings as a function of bath temperature.

T (°C)	*w* (mg)	Re (at%)	Ir (at%)	Ni (at%)	FE (%)	*h* (μm)
50	28.1	60	0	40	35	10.5
60	38.3	56	0	44	48	14.7
70	39.7	33	13	54	44	16.3
80	36.1	32	14	54	39	14.8
90	40.8	34	14	52	44	16.4

Note: pH = 8.0, deposition time 1 h. *w* is the gained mass, *h* is the thickness of the coating.

The effect of bath temperature on the crystallographic structure of the deposits is shown in Fig. 6. For the lowest temperature of 50°C, the halo at ~42.5° indicates an amorphous phase with a chemical composition of ca. $Re_{0.6}Ni_{0.4}$ (Fig. 6a). The formation of the metastable amorphous phase may be attributed to the high Re-content, absence of Ir, and the relatively low deposition temperature, which results in slower diffusion and higher activation energy for crystallization. When the temperature was raised to 60°C, sharp reflections related to hcp-Ni (space group $P6_3/mmc$, JCPDS file #45–1027), and possibly also to hexagonal Ni_2H (JCPDS #33–0606), appeared in addition to the halo related to the amorphous Re-Ni phase (Fig. 6b). Post-electrolysis decomposition of the nickel hydride to pure Ni would induce residual

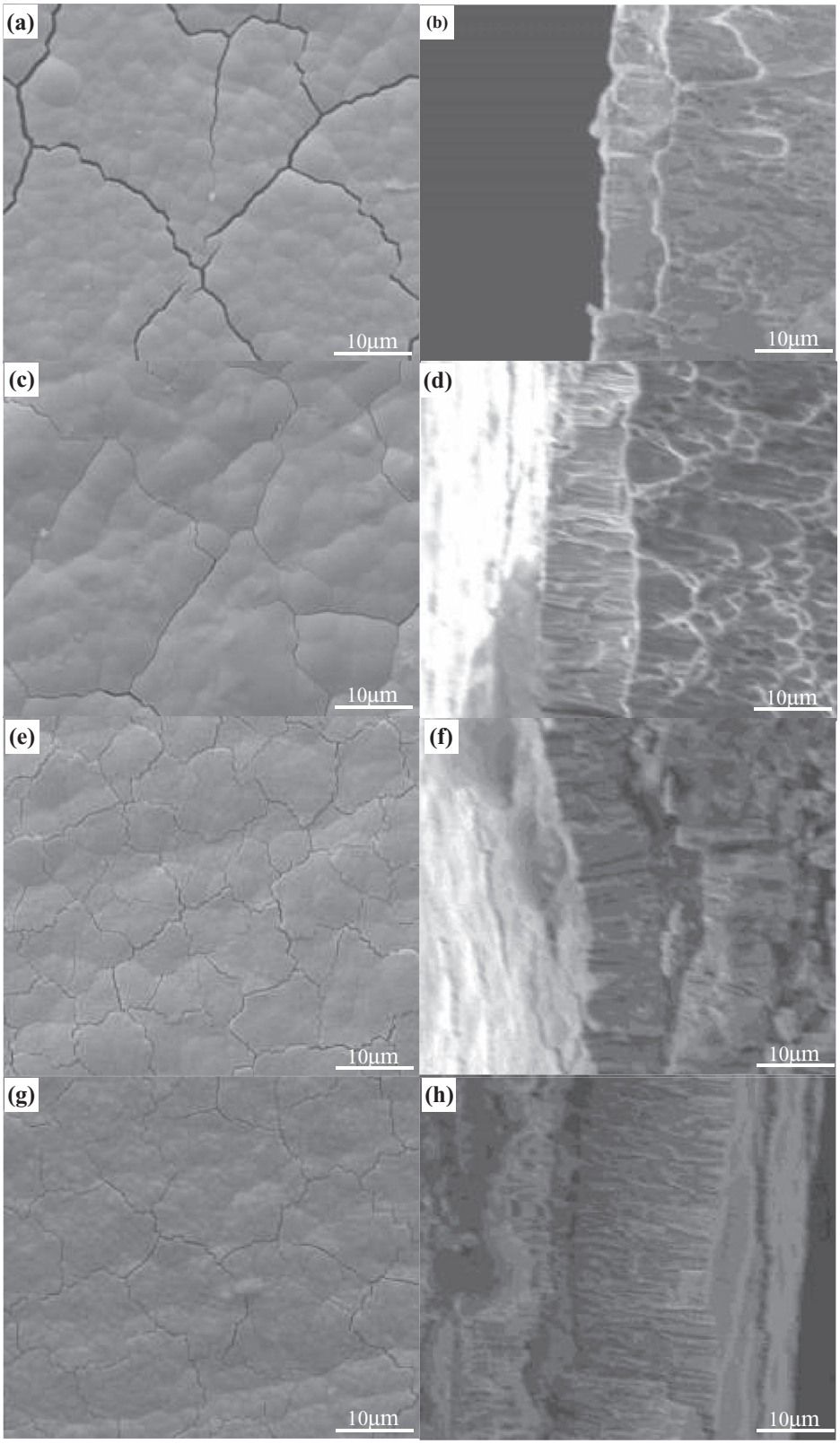

Figure 5. ESEM images of the top surfaces and fracture surfaces of Re-Ir-Ni coatings deposited at different temperatures. (a, b) $T = 50^{\circ}$C, (c, d) $T = 60^{\circ}$C, (e, f) $T = 80^{\circ}$C, (g, h) $T = 90^{\circ}$C. The pH was 8.0.

stresses, which may be the cause of the cracking observed in Fig. 5c. According to the Re-Ni phase diagram, there is an extensive mutual solubility of Re and Ni, and absence of intermetallic compounds. With further increasing temperature (70–90°C), the crystallographic structure of the coatings was similar to that of the coatings formed at $T = 70^{\circ}$C and pH = 4.0–8.0 (see Fig. 3). These coatings had a nanocrystalline structure of hcp-Ni along with hcp-$Ir_{0.4}Re_{0.6}$ (space group $P6_3/mmc$, JCPDS #97–010–4549 or #01–071–9295). The atomic radii of Re and Ir are very close. Thus, Ir atoms can occupy substitutional sites of the hexagonal Re host lattice, forming a solid solution of Re-Ir-based alloy. The phases reported herein were observed in our previous work too,[9] and analysed in detail.

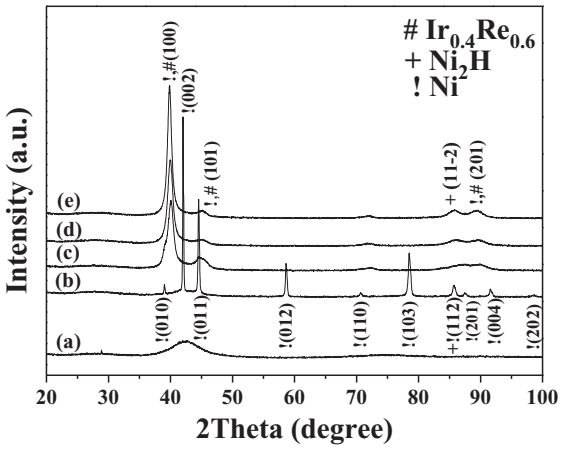

Figure 6. XRD patterns from Re-Ir-Ni coatings deposited at different temperatures. (a) $T = 50°C$, (b) $T = 60°C$, (c) $T = 70°C$, (d) $T = 80°C$, and (e) $T = 90°C$.

Conclusions

In this study, Re-Ir-Ni alloy coatings were electroplated from citrate-containing aqueous solutions. The effects of pH and temperature on the faradaic efficiency (FE), chemical composition, surface morphology and crystallographic structure of the coatings were determined. The following conclusions were made:

1) As the pH is increased from 2.0 to 8.0 (at $T = 70°C$), the FE, partial current densities for deposition of the three metals, and deposition rate increase.
2) The highest Re-content is obtained at pH = 2.5, in a 82Re-8Ir-10Ni alloy (numbers represent at%). A decrease of pH, to 2.0, results in the formation of a 70Re-18Ir-12Ni alloy that, while containing less Re and slightly more Ni, may provide a better high-temperature oxidation resistance due to the higher Ir content.
3) At pH = 2.0, the coating consists of an amorphous phase, and no surface cracks are observed. When the pH is raised to 4.0 and above, crystalline phases (including hydrides) form, and both columnar crystals and micro-cracks are observed.
4) The bath temperature (at pH 8.0) affects the surface crack density and the size of the grains that form the mesoscopic colonies at the outer surface. At the two lowest temperatures studied herein (50 and 60°C), no codeposition of Ir is observed. The phase composition of the coating changes from amorphous Re-Ni at 50°C; to amorphous Re-Ni, hcp-Ni and hexagonal Ni_2H at 60°C; to hcp-$Ir_{0.4}Re_{0.6}$, hcp-Ni and hexagonal Ni_2H at higher temperatures.
5) The pH for crack-free deposit with high (Re+Ir)-content was found to be in the range of 2.0–2.5 at 70°C. However, the FE was the lowest and the alloy was very thin. A temperature of 70°C would seem to be the best choice for electroplating of Re-Ir-Ni at pH 8.0, since above it heavy evaporation and a relatively high density of surface cracks are observed, while below it Ir is not codeposited.
6) While the effect of temperature in chemical kinetics is rather straightforward, this is not the case here, because there are at least four reactions taking place in parallel – the deposition of the three metals and hydrogen evolution. Since the Gibbs energies of activation are not known, it is impossible to predict which reaction would become more dominant than the others as the temperature is varied. Hence, more experimental data are needed to optimize this system.

Acknowledgments

This research was conducted with financial support from the U.S. Air Force Office of Scientific Research (AFOSR, grant number #FA9550-10-1-0520) as well as from the Israel Department of Defense (grant number #4440258441). The authors thank Dr. Zahava Barkay and Dr. Yuri Rosenberg from the Wolfson Applied Materials Research Center for their help in ESEM/EDS and XRD characterization, respectively, and Mario Levenshtein for his help in the preparation of copper samples and electroplating system apparatus. Wangping Wu is thankful to the Pikovsky Valazzi fund, Tel-Aviv University, for providing him with a postdoctoral scholarship.

References

1. N. Eliaz and E. Gileadi, in *Modern Aspects of Electrochemistry*, Editors, C. G. Vayenas, R. E. White, and M. E. Gamboa-Aldeco, Springer, **42**, 191 (2008).
2. A. Naor, N Eliaz, E Gileadi, and S. R. Taylor, *The AMMTIAC Quarterly*, **5**(1), 11 (2010).
3. Y. G. Tong, S. X. Bai, H. Zhang, and Y. C. Ye, *Appl. Surf. Sci.*, **261**, 390 (2012).
4. A. Naor, N. Eliaz, and E. Gileadi, *Electrochim. Acta*, **54**, 6028 (2009).
5. A. Naor, N. Eliaz, and E. Gileadi, *Electrochem. Soc. Trans.*, **25** (29), 137 (2010).
6. A. Naor-Pomeranz, L Burstein, N. Eliaz, and E. Gileadi, *Elecrochem. Solid-State Lett.*, **13**(12), D91 (2010).
7. A. Naor, N. Eliaz, and E. Gileadi, *J. Electrochem. Soc.*, **157**(7), D422 (2010).
8. A. Naor-Pomerantz, N. Eliaz, and E. Gileadi, *Electrochim. Acta*, **56**(48), 6361 (2011).
9. M. Cohen-Sagiv, N. Eliaz, and E. Gileadi, *Electrochim. Acta*, **88**, 240 (2013).
10. O. Berkh, N. Eliaz, and E. Gileadi, *J. Electrochem. Soc.*, **161**(5), D219 (2014).
11. O. Berkh, A. Khatchatouriants, N. Eliaz, and E. Gileadi, *J. Electrochem. Soc.*, **161**(12), D632 (2014).
12. B. A. Rosen, E. Gileadi, and N. Eliaz, *J. Electroanal. Chem.*, **731**, 93 (2014).
13. A. Duhin, A. Inberg, N. Eliaz, and E. Gileadi, *Electrochim. Acta*, **56**(26), 9637 (2011).
14. A. Duhin, A. Rozenblat-Raz, L. Burstein, A. Inberg, D. Horvitz, Y. Shacham-Diamand, N. Eliaz, and E. Gileadi, *Appl. Surf. Sci.*, **313**, 159 (2014).
15. W. P. Wu, X. Lin, Z. F. Chen, Z. Chen, X. N. Cong, T. Z. Xu, and J. L. Qiu, *Plasma Chem. Plasma Process.*, **31**(3), 465 (2011).
16. Z. F. Chen, W. P. Wu, and X. N. Cong, *J. Mater. Sci. Technol.*, **30**(3), 268 (2014).
17. Z. F. Chen, W. P. Wu, H. Cheng, Y. Liu, S. M. Wang, and R. J. Xue, *Acta Astronaut.*, **66**(5–6), 682 (2010).
18. W. P. Wu, Z. F. Chen, H. Cheng, L. B. Wang, and Y. Zhang, *Appl. Surf. Sci.*, **257**(16), 7295 (2011).
19. J. R. Davis (Ed.), *ASM Specialty Handbook: Heat-Resistant Materials, ASM International*, Materials Park (1997).
20. B. D. Reed, J. A. Bigalow, and S. J. Schneider, *Mater. Manufact. Process.*, **13**(10), 757 (1998).
21. R. H. Tuffias, *Mater. Manufact. Process.*, **13**(10), 773 (1998).
22. http://www.nasa.gov/centers/glenn/pdf/168206main_CenterResume.pdf (accessed 19.8.14).
23. J. R. Vargas Garcia and T. Goto, *Mater. Trans.*, **44**(9), 1717 (2003).
24. K. Mumtaz, J. Echigoya, and M. Taya, *J. Mater. Sci.*, **28**(20), 5521 (1993).
25. W. P. Wu, Z. Chen, X. Cheng, and Y. Wang, *Nucl. Instr. Meth. Phys. Res. B*, **307**, 315 (2013).
26. L. A. Zhu, S. X. Bai, H. Zhang, and Y. C. Ye, *Appl. Surf. Sci.*, **282**, 820 (2013).
27. T. Jones, *Metal Finishing*, **102**(6), 87 (2004).
28. F. Wu, H. Murakami, Y. Yamabe-Mitarai, H. Harada, H. Katayama, and Y. Yamamoto, *Surf. Coat. Technol.* **184**(1), 24 (2004).
29. J. Hatswell, *Platinum Metals Rev.*, **10**, 59 (1966).
30. T. Ohsaka, K. Hirano, and S. Imbayashi, *Electrochem. Solid-State Lett.*, **13**(8), D65 (2010).
31. L. E. Netherton and M. L. Holt, *J. Electrochem. Soc.*, **98**(3), 106 (1951).
32. O. Yu. Zelenin, *Russ. J. Coordination Chem.*, **33**(5), 346 (2007).
33. J. J. Vajo, D. A. Aikens, L. Ashiley, D. E. Poeltl, R. A. Bailey, H. M. Clark, and S. C. Bunce, *Inorg. Chem.*, **20**(10), 3328 (1981).
34. E. Budevski, G. Staikov, and W. J. Lorenz, "Electrochemical Phase Formation and Growth: An Introduction to the Initial Stages of Metal Deposition," VCH, Weinheim, (1996).
35. M. Volmer and A. Weber, *Z. Physik. Chem.*, **119**(3–4), 277 (1926).
36. R. Weil, *Annu. Rev. Mater. Sci.*, **19**, 165 (1989).
37. J. W. Dini, "Electrodeposition: The Materials Science of Coatings and Substrates," Noyes Publications, New Jersey, 141 (1993).
38. M. Schwartz, "Deposition from aqueous solutions: An overview," In R. F. Bunshah (Ed.), *Handbook of Deposition Technologies for Films and Coatings – Science, Technology and Applications*, William Andrew Publishing, London, 506 (1994).
39. A. K. N. Reddy, *J. Electroanal. Chem.*, **6**(2), 141 (1963).